Version of Record: https://www.sciencedirect.com/science/article/pii/S1526612520301171
Manuscript_c4d5fe7aecd60bbeabebb1d380c93cc2

Correlation Approach for Quality Assurance of Additive Manufactured Parts Based on Optical Metrology

Xiao Zhang[a], Yi Zheng[b], Vignesh Suresh[b], Shaodong Wang[a], Qing Li[a], Beiwen Li[b*], Hantang Qin[a,*]

[a] *Industrial and Manufacturing Systems Engineering Department, Iowa State University, Ames, Iowa, 50011, USA*
[b] *Mechanical Engineering Department, Iowa State University, Ames, Iowa, 50011, USA*

* Corresponding author. Hantang Qin, Tel.: +1-515-294-1248. *E-mail:* qin@iastate.edu

Abstract

Surface topography and surface finish are two significant factors for evaluating the quality of products in additive manufacturing (AM). AM parts are fabricated layer by layer, which is quite different from traditional formative or subtractive methods. Despite rapid progress in additive manufacturing and associated optical metrology for quality control and in-situ monitoring, limited research has been conducted to investigate the reliability of 3D surface measurement data. The surface topologies scanned by multiple optical systems demonstrated significant differences due to varying sampling mechanisms, resolutions, system noises, etc. The 3D datasets should be trustworthy in order to extract parameters for quality assurance or feedback control from 3D surface measurements. In this paper, we set up new standards to evaluate the reliability of 3D surface measurement data and analyze the variation in the topographical profile. In this study, two non-contact optical methods based on Focus Variation Microscopy (FVM) and Structured Light System (SLS) were adopted to measure the surface topography of the target components. The two optical metrology systems generated two entirely different point cloud datasets. Statistical methods were applied to test the difference between the data obtained from the two systems. By using data analytics approach for comparison, it was found that the surface roughness estimated from the point cloud data sets of FVM and SLS has no significant difference, though the point cloud data sets were completely different. This paper provides standard validation approach to evaluate the plausibility of metrology data from in-situ real-time surface analysis for process planning of AM.

Keywords: surface roughness; additive manufacturing; 3D scanning; point cloud data; statistical analysis.

1. INTRODUCTION

Additive manufacturing (AM), widely known as 3D printing, involves manufacturing of parts by building them layer by layer. It has developed rapidly in recent years, demonstrating its capability in a wide range of applications and many industries such as automotive, aerospace, and consumer products [1]. There are several advantages of AM processes compared to conventional subtractive manufacturing processes. Complex shapes with many intricate features can be made easily by AM processes [2]. Also, the material wastage is less compared to that of subtractive manufacturing [3]. Given that AM could be the future, it became necessary to inspect the quality

of the parts being made. The inherent problem in the AM parts is their strength, which was dependent on the surface profile of each layer being added [4]. In addition, tool traverse path impacts the part profiles significantly, leading to many researchers focusing on the characterization of surface roughness of 3D printed components [5-9].

Surface roughness denotes smoothness and quality of a surface. It is one of the most critical factors to assess the quality of manufactured components in the industry. The surface roughness measurement techniques could be classified into two categories: contact methods and non-contact methods [10]. For contact methods, a stylus was the most popular instrument for surface roughness measurement. The stylus runs perpendicularly to the surface of a fixed part along a straight line, and surface roughness could be calculated based on *x/z* position information of this line. For commercial application, Rank Taylor Hobson introduced the first instrument in Leicester, England called Talysurf [11]. By moving a probe along a surface, an analog electrical signal was generated when the probe vibrates with the surface variation. After obtaining this signal, the centerline average roughness (CLA) was calculated by a simple analog computer. This procedure eventually became the standard for measuring surface roughness [12]. Veniali et al. used a Taylor Hobson Talysurf Form Plus profilometer to measure a fused deposition model (FDM) part [13]. They found that the profile was effective in describing the micro-geometrical surface of FDM prototypes. However, the contact surface roughness method had inevitable limitations. Soft parts might be damaged during the measurement process because of the contact made by the stylus during the measurement process.

Non-contact methods have been developed to overcome this issue. X-ray computed tomography method applied the characteristic of X-ray to calculate the surface roughness, A. Thompson et al. [14] reviewed studies using X-ray computed tomography (CT) technology to build up 3D surface maps of AM parts. Laser scanning could provide topography information with high accuracy which has attracted the attention of many researchers [15,16]. Other than laser scanning system, ultrasonic methods could also detect the surface roughness, which uses an ultrasonic transmitter for emitting sound pulses to the surface, based on the Doppler effect, the surface roughness was calculated [17-19]. Various microscope systems provided the advantages of the non-contact optical profiler method without damaging the part, fast response and higher accuracy. Poon et al. [20] compared stylus profiler, atomic force microscope (AFM) and non-contact optical profiler to measure the surface roughness. Scanning electron microscopy [21], digital fringe projection [26] and stereomicroscope system [22] have been used for surface measurements. Neural network [23], digital image magnification technique [24], modified binary speckle image and adaptive optics [25] have been adopted for advanced image processing and data processing. Among these techniques, the structured light system provided fast response, high accuracy way for measuring the surface roughness. Zhang et al. [26] were able to utilize fringe projection techniques to perform in-situ inspection for laser powder bed fusion. Focus variation microscopy is another high accuracy metrology system that can be used for surface quality inspection in additive manufacturing [27]. In this work, we use these two metrology systems as testbeds to identify if the two different methods have consistent surface roughness values or the same surface.

Optical techniques are the preferred non-contact methods to measure the surface topography and calculate the surface roughness. Optical methods could analyze the surface topography with high efficiency based on different image processing methods, especially with the help of high performance computing nowadays. However, with different optical systems and light sources, there were still several considerable differences. In longitudinal turning process, modeling and prediction of surface roughness on parameters such as R_a, R_p, and R_z were compared to indicate the condition of surface roughness [28]. However, limited research has been done to determine whether the performance of different optical systems was consistent. Without such knowledge, the trustworthiness of data extracted from different metrology systems could not be determined. In order to compare the systems the same sample surface should be analyzed with different measurement systems. The focus of this research will be on the comparison of one surface roughness parameter to resolve the potential conflict between manufacturer and customer who use their own different optical system to check the quality of the manufactured parts. Our null hypothesis was that the surface topography from different systems based on point cloud data analysis followed the same distribution. If failing to reject the null hypothesis, it indicated that the surface roughness of the 3D-printed plastic or metal objects based on different optical systems were reliable, which could be used to compare the quality of different 3D-printed objects. Objects with better quality usually have lower surface roughness. If the two systems conflicted with each other, further work should be conducted to investigate the cause of difference between the two systems.

Based on the point cloud data generated from each system, an algorithm was developed to align the two groups of topography information. In order to perform statistical comparison, the surface roughness was estimated from each point cloud data set. The Structured Light System (SLS) was employed to measure surface roughness of the additive printed part. In this work, since Focus Variation Microscopy (FVM) system has higher precision, it was used to verify the resolution of the SLS system, which helped the system to realize the potential reliable real-time surface measurement of 3D printed part during the manufacturing process. By scanning the topography information of each layer during the printing process, overall information of the surface roughness for a particular 3D printed part was achieved.

2. METROLOGY SETUP AND MEASUREMENT METHODS

2.1. Focus Variation Microscopy (FVM)

The setup of the FVM is shown in Figure 1a. The resolution of the lens used was 1.1 µm, and the field of view was 2-3 mm square. Based on FVM, the topographical information of the additive manufactured part is demonstrated in Figure 1b. The height of this metal filament (from the top of the metal filament to the bottom of the metal filament, peak-to-peak value) was 0.224 mm; the field of view used was 3 mm square. The focus variation microscopy was used to verify the accuracy of structured light system (which has a lower depth resolution).

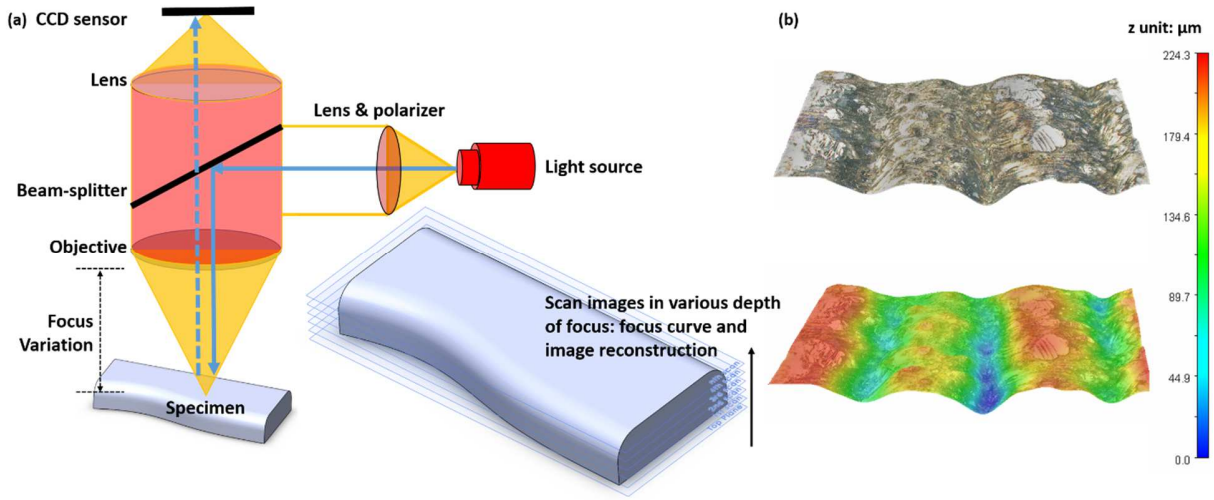

Figure 1: (a) Schematic of Focus Variation Microscopy (FVM), and (b) FVM image of the additive manufactured metal part with constructed 3D data.

2.2. Structured Light System (SLS)

As shown in Figure 2a, the Structured light system (SLS) used in this paper was composed of the unit (A), a camera capturing images; unit (B), and a real-world 3D object; unit (C), a projector projecting fringe patterns. Fringe patterns were projected to object, and distorted phase lines were captured by the camera for 3D reconstruction. For establishing the pixel correspondence between the camera and the projector, we used the carrier phase information by implementing the least-square phase shifting algorithm [29].

The least-square phase shifting algorithm could be mathematically described as Equations 1-2. I' represented the average intensity, I''represented the intensity modulation and $\emptyset$ was the phase obtained after solving the phase-shifted patterns. Since $\emptyset$ was computed by an arctangent function, phase jumps of 2π would occur. To remove the 2π phase discontinuities, an unwrapping process was done. Unwrapping was achieved by adding or subtracting multiples of 2π at the locations $k(u,v)$ where there was a discontinuity, to obtain the absolute phase $\Phi(u,v)$.

$$I_i(u,v) = I'(u,v) + I''(u,v)\cos[\emptyset(u,v) + 2i\pi/N] \quad (1)$$

$$\emptyset\,(u,v) = -tan^{-1}\left[\frac{\sum_{i=1}^{N} I_i \sin(\frac{2i\pi}{N})}{\sum_{i=1}^{N} I_i \cos(\frac{2i\pi}{N})}\right] \quad (2)$$

$$\Phi(u,v) = \emptyset(u,v) + k(u,v) \times 2\pi \quad (3)$$

After obtaining the phase map, we adopted a calibration-based 3D reconstruction algorithm [29] to convert the phase map Φ into $3D(x,y,z)$. The test system consisted of a digital-light-processing (DLP) projector and a camera. The camera was attached to a telecentric lens with a magnification rate of 0.486. The resolution of the camera was set to 1280 × 960 pixels. The projector had a 912 × 1140 pixels resolution. We used 18 step phase-shifted patterns for phase

retrieval. Figure 2b shows the sample that was scanned using SLS and reconstructed 3D image (same part as Figure 1b, but different sizes for field of view and resolutions).

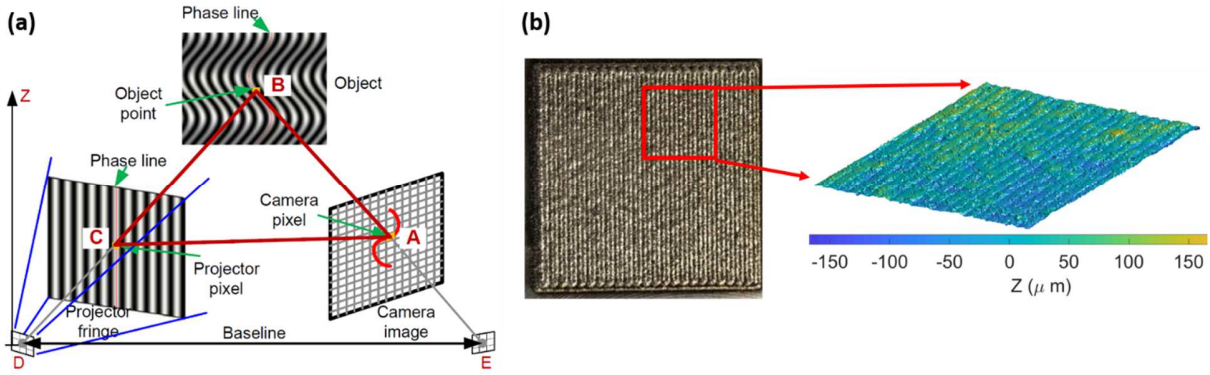

Figure 2: (a) Schematic drawing of the SLS system, and (b) photograph and reconstructed 3D SLS geometry of the metal sample.

3. ANALYTIC APPROACH FOR 3D SURFACE MEASUREMENT

An AM machine could be equipped with a wide variety of optical sensing platforms based on specific manufacturing needs (e.g., repeatability, data sampling resolution). The problem was that different optical sensing techniques and systems tended to produce data with notable disagreement. Systematic approaches that could perform correlation analysis across sensing platforms were essential for obtaining reliable data. In this study, we developed a standard procedure for comparing the data from different optical metrology systems. The problems and approaches were discussed in details in the following sections.

3.1. Extraction Algorithm for Cross-section Profile

An additive manufactured metal sample (as shown in Figure 2b) was used for the measurement and data collection. The results were collected separately from FVM and SLS. Both systems captured the surface topography in the format of point cloud data. The resolution of the structured light system was 10 µm. The scanned area of the SLS was larger than that of FVM. In order to compare the results from the two systems, the scanned zone from both of the systems should be the same. Another challenge was that the data collected from the FVM system was not aligned with the SLS system, so it was difficult to ensure that the cross-sections extracted from the two-point cloud datasets correspond to the same location. Therefore, as a first step, the point cloud datasets from the FVM system and SLS system should be matched and.

Iterative Closest Point (ICP) algorithm [30, 31] was applied to match and align each point from one point cloud data set to its corresponding point in the other point cloud data set. The ICP algorithm took two-point clouds (m and s) as input and returned the rigid transformation (rotation matrix R and translation vector T) that best aligned the two point clouds. If the point cloud data from SLS was denoted by s and the one from FVM was m, the point cloud data could be matched

by transforming either of those. The new point cloud dataset (corresponding to FVM) n can be expressed as:

$$n = R * m + T \quad (4)$$

R and T were the rotation and translation matrices for aligning the point cloud data from FVM with SLS. In this way, both the point cloud data sets would be in the same coordinate system, and the corresponding points from the two systems would be aligned. Note that the point cloud data from FVM is denser than the one from SLS since FVM has a higher resolution. Another observation is that the spatial range of the FVM data is smaller and included in the one of SLS. To achieve finding the corresponding points, our strategy is that we make sure all the points of FVM can find their correspondence. In this case, correspondences can be many-to-one mappings. Therefore, the points that are overlapped in the same scanning area between FVM and SLS are taken into consideration for ICP alignment. By this means, ICP can correctly align the two sets of point cloud data with distinct densities and spatial ranges. In addition, when we use the metrology systems to measure the sample, we are clear about the approximate orientation and the position of the obtained point cloud data based on the knowledge of both systems, therefore we are able to provide a roughly correct initial alignment. Then, the ICP algorithm refines it iteratively, which ensures that the final alignment is accurate, and the correct corresponding cross-sections are compared. To extract the required cross-section, the points that were closest to this required cross-section could be obtained using a k-nearest neighbor search algorithm [29]. The distance *d* of those points to the point (in the chosen cross section) was given by Equation 5.

$$d = (\sqrt{(x_1 - x)^2 + (y_1 - y)^2}) \quad (5)$$

(x_1, y_1) were the points in the chosen region and (x, y) was the point on the required cross-section. The distance between all the closest points was obtained, and the Gaussian model in Equation 6 was used to provide the weights for all the chosen points. Weights were assigned based on the perpendicular distance from the point to the cross section. The i and j were the indices for the points x and y.

$$f(i,j) = \frac{1}{\sigma\sqrt{2\pi}} e^{-\frac{d^2}{2\sigma^2}} \quad (6)$$

The 2D cross-sections extracted from the point cloud data of SLS and FVM are shown in Figure 3a-b. Note that the orientation of the cross-section is perpendicular to the printing direction. The cross-section along this direction provides much useful information such as bead width and layer height, which can be applied for printing quality assessment. From the extracted cross-sections, various surface roughness parameters could be calculated. There were a variety of approaches to quantify the surface roughness, among them the Roughness Average R_a was the most widely used measurement in industry. In a cross-section of an object, define z_i to be the vertical coordinate of a point on the cross-section, where i was the index of scanned points on the selected line. z_0 was defined as the mean of z_i from all cross sections. The arithmetic average of

the surface roughness profile R_a calculated using Equation 7 at multiple slicing locations was demonstrated in Figure 3c.

$$R_a = \frac{1}{n}\sum_{i=1}^{n} |z_i - z_0| \quad (7)$$

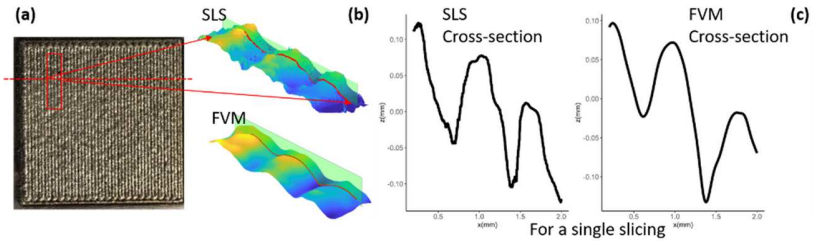

(c)

Slicing No.	R_a / µm SLS	R_a / µm FVM	Difference %
10	48.55	45.45	6%
15	44.13	50.91	14%
20	41.94	54.99	32%
25	42.07	57.77	36%

Figure 3: Image of the additive manufactured metal part: (a) 3D profiles based on SLS and FVM, (b) 2D cross-section profiles extracted at red lines, and (c) differences in R_a values at different slicing locations.

As we can see from Figure 3c, the percentage differs based on the calculated R_a was up to 36%. With such a big difference, it was difficult to identify the uniformity of the two datasets. If the data were to be used as a decision-making factor for feedback control or quality check, the results could generate significant ambiguities. In order to test the reliability of the 3D surface measurement data, two approaches based on 2D cross-section data analysis and direct 3D data comparison were developed.

3.2. Statistical Approach for 2D Cross-section Analysis

After extracting the data from two different 3D optical systems, the following statistical algorithms were used to compare the roughness parameter.

3.2.1. Shapiro-Wilk Test

The Shapiro-Wilk test [34] was used to check if a random sample $X = \{x_i | \, i = 1,2,\ldots,n\}$ came from a normal distribution. The null hypothesis of the Shapiro-Wilk test was that X followed a normal distribution. The test statistic was in Equation 8.

$$W = \frac{(\sum_{i=1}^{n} a_i x_{(i)})^2}{\sum_{i=1}^{n}(x_i - \bar{x})^2} \quad (8)$$

In Equation 8, $x_{(i)}$ was the $i^{th\ the}$ smallest value among all $x_i's$, $\bar{x}$ was the sample mean, and a_i was a coefficient related to the standard normal distribution. If W was greater than the critical threshold, the normality assumption of X should be rejected.

3.2.2. Paired t-test

The paired t-test [33] was used to compare two population means where there were two samples, and the observations from these two samples could be paired. Assume we had two

dependent random samples $X = \{x_i | \ i = 1, 2, \ldots, n\}$ and $Y = \{y_i | \ i = 1, 2, \ldots, n\}$ from normal distributions with the same standard deviation and means $\mu_1$and μ_2. $x_i$and y_i were observed from the same entity, $i = 1, 2, \ldots, n$. The null hypothesis and alternative hypothesis were H_0 and H_1, where H_0: $\mu_1 = \mu_2$ and H_1: $\mu_1 \neq \mu_2$. The t-statistic was calculated in Equation 9.

$$t = \frac{\sum_{i=1}^{n}(x_i - y_i)}{\sqrt{\frac{1}{n(n-1)}\sum_{i=1}^{n}(x_i - y_i)^2}} \quad (9)$$

If $|t|$ was greater than the 97.5th percentile of the t-distribution with $n - 1$ degrees of freedom, which meant the p-value was less than 0.05, we rejected the null hypothesis and concluded that X and Y were from two different distributions ($\mu_1 \neq \mu_2$).

3.2.3. Wilcoxon Signed-rank Test

If two samples $X = \{x_i | \ i = 1, 2, \ldots, n\}$ and $Y = \{y_i | \ i = 1, 2, \ldots, n\}$ did not come from normal distributions; Wilcoxon signed-rank test [36] should be used. There are many non-parametric statistical tests that compared two samples without the requirement of normal assumption, such as Kolmogorov–Smirnov test [40], Wilcoxon rank sum test [41] and Wilcoxon Signed Rank Test. Wilcoxon signed-rank test was the most suitable one in this study, because it is particularly for matched pair samples and R_a measured by SLS and FVM were exactly matched pair sample. The steps of the Wilcoxon signed-rank test [36] was as follows in Figure 4.

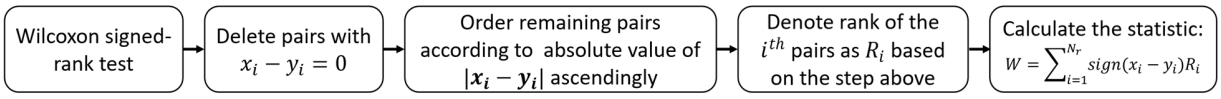

Figure 4: Wilcoxon test flowchart

In the last step, N_r was 25 in the study conducted in this paper, and $sign(x)$ was an indicator function. If x was positive, $sign(x)$ would be 1; if x was negative, $sign(x)$ would be -1. If the calculated statistic W was greater than the critical value of $W_{critical,\,N_r}$, the null hypothesis would be rejected, and we could conclude that X and Y were from a different distribution.

A suitable test would be used according to the property of the data. If the normal assumption (R_a the difference from the two systems) was violated, nonparametric methods would be preferred. Otherwise, the paired *t*-test would be used. If the surface roughness calculated using the two datasets from the same part had no significant difference, there would be no evidence against the assumption that the structured light system and the focus variation microscopy had the same performance on scanning. The working flow, as illustrated in Figure 5 below.

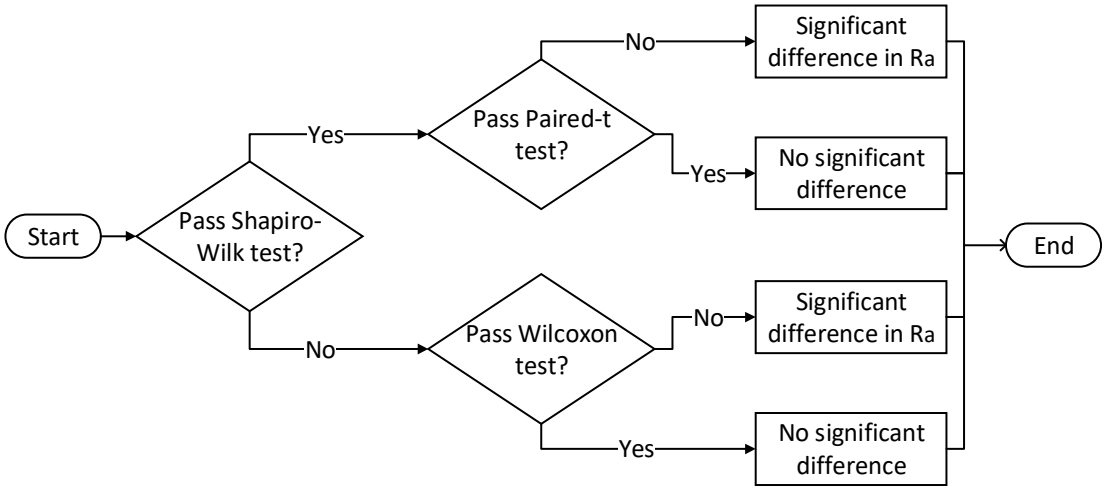

Figure 5: Workflow of statistical tests

3.3. Analytical Approach for 3D Data Comparison

In the previous section, data comparison among 2D cross-section profiles was established, which provided an effective method to evaluate data plausibility in the 2D domain (e.g., comparing profilometry and scanned 3D datasets). However, extracting 2D data from 3D datasets resulted in information loss, which would be a countermarch to the effort for future 3D analysis. To address this issue, instead of comparing R_a values, we developed the approach based on Pearson's Correlation Coefficient (PCC) [37] for a direct comparison of surface topology data in 3D space. Essentially, PCC was a measure of the linear correlation between two variables, which took values between -1 and 1, where 1 indicated total positive linear correlation, 0 no linear correlation, and -1 total negative linear correlation.

Once multiple 3D datasets were registered through iterative-closest-point and k-nearest neighbor resampling, consistency evaluation among the registered 3D data obtained from different optical systems could be performed. Therefore, the hypothesis was that if two 3D datasets were measured from the same surface, they should pass the PCC examination. The computation procedure of PCC was explained below.

The first step was to convert the 3D point matrices into 2D depth images with well-aligned mesh grids. Supposing we had two converted depth images D_1 and D_2 with a dimension of M × N from two different 3D data, the depth images would then be converted into vectors v_1 and v_2 with a length of M × N in preparation for calculation of PCC using Equation 10.

$$PCC = \frac{(v_1-\bar{v}_1)\cdot(v_2-\bar{v}_2)}{\sqrt{(v_1-\bar{v}_1)\cdot(v_1-\bar{v}_1)}\sqrt{(v_2-\bar{v}_2)\cdot(v_2-\bar{v}_2)}} \qquad (10)$$

where $\bar{v}_1, \bar{v}_2$ were the mean of the two vectors correspondingly, and "·" was the inner product. If two depth images were similar, the converted vectors should have a strong linear correlation with the PCC value close to one.

4. RESULTS AND DISCUSSION

We would like to point out that p-values and statistical values in this study were a factor to identify differences among datasets; however, in the practical testing of this study, we also carefully reviewed the physical data along with the statistical significance to analyze the results. A statistically significant result proved the null hypothesis (no difference between measured outcomes). There has been a debate of statistical significance recently, arisen from the pharmacy and clinic testing [36, 37], indicating some false conclusions. In our study, all data were validated both physically and statistically, to avoid misuse of statistical significance.

4.1. Data Analysis of 2D Cross-Section

The cross-section images from FVM and SLS of the metal part are shown in Figure 5. The cross-section of FVM and the SLS were not precisely the same, but have the same trend, which as reasonable. A total of 50 (25 from SLS and 25 from FVM) cross-section profiles were extracted from both of the point cloud datasets. For each cross-section, there were 1801 points to calculate the R_a value using Equation 7, and the results are shown in Figure 6a-b. All the cross-sections had the same horizontal length of 2 mm. In the manufacturing process of selective laser melting of 361L stainless steel, surface roughness R_a was measured for determining material removing rate [42]. In cutting process, the relationship of surface roughness parameter R_a and spindle speed, feed-rate and machining time was investigated [43]. In surface defect machining processing, surface roughness R_a of AISI 4340 part was calculated to prove this technique could manufacturing parts which satisfy ASTM standards [44]. In order to determine whether the performance of the two systems was similar, we compared the R_a values obtained from the cross-sectional plots of the two systems. The Shapiro-Wilk [34] test was conducted to determine whether the difference between the two samples follows the normal distributions or not. If the normality assumption was accepted, the paired *t*-test [35] would be used to test the population means of the two datasets. Otherwise, if the datasets violated the normality assumption, a non-parametric method, the Wilcoxon signed-rank test [36], would be used.

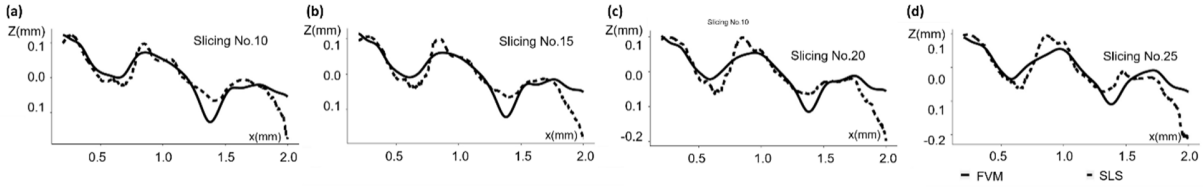

Figure 5: Cross-section of the FVM and SLS based on scanned point cloud datasets

Table 1. Surface roughness data from FVM and SLS

Slicing No.	*R_a _ FVM (μm)*	*R_a _ SLS (μm)*	*Slicing No.*	*R_a _ FVM (μm)*	*R_a _ SLS (μm)*
1	42.3917	53.4998	14	53.7451	49.1922
2	50.2008	44.1331	15	44.1254	50.9112
3	52.8794	50.3658	16	41.7624	56.1287
4	52.7942	43.1504	17	53.6251	44.0176
5	43.1264	52.4136	18	51.6375	43.2483
6	54.2452	46.6477	19	54.1086	45.2432
7	42.415	57.3948	20	41.9405	54.9878
8	41.8247	57.202	21	53.3152	50.1836
9	46.8622	46.9997	22	52.4384	50.3091
10	48.5498	45.4499	23	51.5983	50.7457
11	54.082	48.05	24	45.369	49.0713
12	42.7874	55.9695	25	42.0667	57.7666
13	52.0042	50.4453			

Table 1 and Figure 6 showed that the R_a difference between the two systems did exist. Sometimes FVM had larger R_a and sometimes it had smaller R_a. It was feasible that R_a from FVM and SLS were fluctuated but balanced. We could not make conclusions by just observing the data visually. Therefore, statistical tests must be performed to compare datasets.

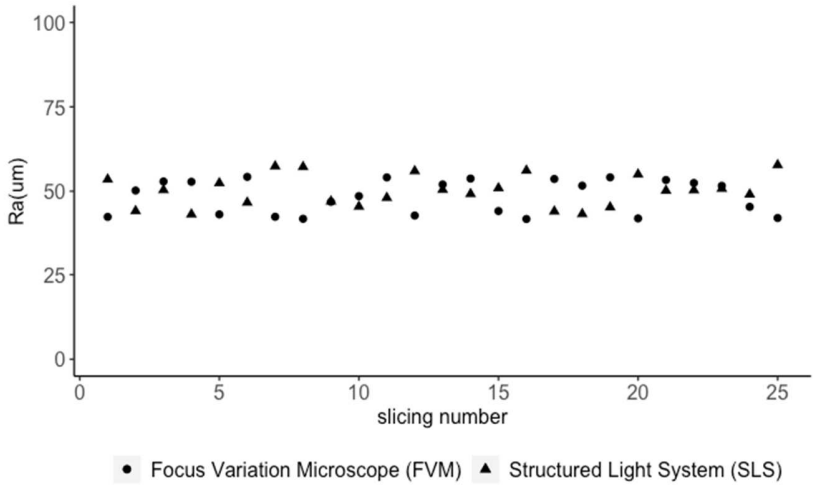

Figure 6: R_a of 25 cross-section samples from the FVM and SLS based on scanned point cloud data (b) statistical test results

Table 2. Statistical test results

Statistical Test	*p-value*
Shapiro-Wilk test	0.007574
Paired t-test	N/A
Wilcoxon signed-rank test	0.4578

The statistical results were shown in Table 2. The null hypothesis of the Shapiro-Wilk test was that the two paired surface roughness datasets followed a normal distribution, while the null hypothesis of the paired t-test and the Wilcoxon signed-rank test was that the two paired surface roughness datasets followed the same distribution. The null hypothesis would be rejected when the p-value of the test is smaller than 0.05, which meant the calculated statistics based on observations were far away from the value required by the null hypothesis. Since the p-value of the Shapiro-Wilk test was 0.007574, which was much smaller than 0.05, we rejected the null hypothesis and concluded that the normality assumption was violated. Therefore, the Wilcoxon signed-rank test was conducted, and its p-value was 0.4578. The p-value was larger than 0.05; hence we did not find clear evidence against the hypothesis that surface roughness based on the two systems were from the same distribution.

(a)

(b)

	SLS Sample 1	FVM Sample 1	SLS Sample 2	FVM Sample 2	SLS Sample 3	FVM Sample 3
SLS Sample 1	1	0.7947	-0.3949	-0.2849	-0.1502	-0.0608
FVM Sample 1	0.7947	1	-0.4017	-0.3317	-0.1359	-0.0630
SLS Sample 2	-0.3949	-0.4017	1	0.6029	0.2664	0.1945
FVM Sample 2	-0.2849	-0.3317	0.6029	1	0.0019	0.1287
SLS Sample 3	-0.1502	-0.1359	0.2664	0.0019	1	0.6635
FVM Sample 3	-0.0608	-0.0630	0.1945	0.1287	0.6635	1

(c)

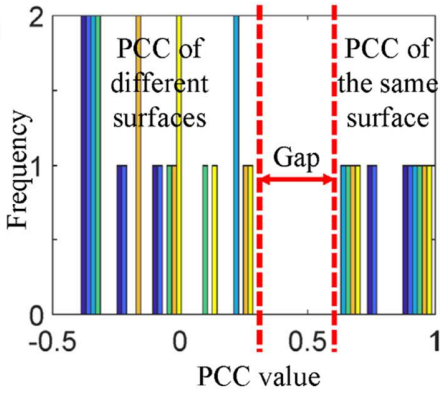

Figure 7. (a) Metal samples from Direct Energy Deposition, (b) computed PCC values and (c) histogram for cross-comparison among different sample surfaces measured by SLS and FVM.

4.2. Data Analysis of 3D Point Cloud Datasets

In this study, SLS and FVM were used to obtain the 3D datasets of three samples fabricated by direct energy deposition, as shown in Figure 7a. The objective was to validate whether the 3D datasets measured from different systems were following the same surface topological distribution. Figure 7b shows the results when using PCC as an indicator for consistency between two 3D datasets obtained from SLS and FVM. It showed that the computed PCC values for the same sample were closer to 1 compared with PCC values for different samples, and the histogram on the right (Figure 7c) clearly showed that a big gap exists for the PCC values computed between the same sample and different samples. Each color in Figure 8c indicates one PCC value of one sample comparison in Figure 7b. The result was promising in identifying the same measured sample from different optical platforms. Therefore, it has been shown that Pearson's Correlation

Coefficient (PCC) was a strong and reliable indicator for the identification of the same measured sample across different optical metrology platforms.

4.3. Contributions of the Approaches

In additive manufacturing, both in-situ inspection and off-line examination are important given that the former activity assists corrective actions in process, and the latter activity ensures low quality products do not go off the production line. In a modern manufacturing environment, a downstream manufacturer may use a different optical system for surface topology inspection than the one used by its upstream manufacturer. The surface landscapes acquired from these systems can have significant disagreements due to different optical principles, sensor noise or spatial sampling. Such disagreement may cause confusions or miscommunication in a cyber-environment where surface data is shared by all members of a manufacturing stream. A practical question will arise regarding how one could rationally evaluate surface roughness given surface data presenting different resolutions in the cloud-manufacturing database. The objective of this research is to identify statistical methodologies for cyber-metrology data correlation and consistency evaluation among multiple stations.

In this study, SLS and FVM were used to obtain the 3D datasets of three samples fabricated by direct energy deposition (as shown in Figure 7a) *Non-damage measurement.* Compared with tactile measurements which typically involve probe touching the sample, instruments used in our method will not directly contact the sample. Thus, the chance of damaging the sample during the measurement process is drastically reduced.

Substitutability. From the statistical tests, we can conclude that the values of R_a measured by both systems are consistent. There are upstream manufacturer and downstream manufacturer in the product cycle. The upstream manufacturer will need to provide the surface roughness information to downstream manufacturer in order to present the product quality to downstream manufacturer. However, downstream manufacturer will also conduct the measurement with their system to get the surface roughness. The measured surface roughness results could be different due to the measurement by different system. Or the reason could even be measuring the wrong sample. This paper used FVM and SLS system to measure the surface roughness of additive manufactured samples and provided the statistical data to compare the *Ra* values. A robust model was provided for the research community and industry to resolve the possible conflicts and misunderstanding of surface roughness.

Potential for in-situ measurement. The SLS system can reach a scanning rate of 30 kHz, so if we implement the system inside an AM machine, the *in-situ* measurement can be achieved. This can create significant values for additive manufacturing. For example, during the manufacturing process, if the SLS system detects an unexpected bump on the certain layer (i.e., the value of R_a is abnormally large), it can automatically inform the system to feed less material on the next layer in the bump location. In this way, the quality of the workpiece can be assured.

5. CONCLUSIONS

There are a few non-contact optical methods that have been applied to calculate the surface roughness of additive manufactured parts based on point cloud data collected. However, the point cloud datasets from different optical methods on the same scanned area demonstrated different point values. Upon slicing, the data demonstrated different cross-section line profiles. Limited research has been conducted to validate whether the point cloud datasets generated from different optical systems are following the same distribution. If not, surface roughness value R_a from different systems would be unreliable.

In this paper, two different optical measurement techniques were used to measure the 3D surface topography of the parts manufactured by AM processes. Statistic methods were applied in the paper that proved that the surface roughness measurements of additive manufactured samples using SLS and FVM system were equivalent. Algorithms have been demonstrated to extract various cross-sections from the point cloud data generated by two systems. The surface roughness parameter, the arithmetic average of roughness profile (R_a) was calculated using the extracted cross-sections. The statistical test has been conducted to compare the two systems, which showed R_a calculated using the cross-sections obtained from both of the systems agreed with each other. Data correlation and consistency evaluation approach was developed for data comparison among point cloud datasets. The PCC value was a reliable indicator for the identification of the same measured sample across different optical metrology systems.

Surface point cloud data from other non-contact optical methods can be validated based on approaches in this work, e.g., laser scanning and acoustic techniques. The future research work of our group is to provide a standard measurement approach for non-contact and real-time quantification of surface roughness and quality assessment of additively manufactured parts, which could pave a way to bring a new standard to AM industry.

Acknowledgments

This paper is based upon work supported by the U.S. Department of Energy's Office of Energy Efficiency and Renewable Energy (EERE) under the Advanced Manufacturing Office Award Number DE-EE0007897, and by Exploratory Research Project grant from Department of Industrial and Manufacturing Systems Engineering (IMSE_ERP) at Iowa State University. Their supports are greatly appreciated.

Declarations of interest

The authors declare that they have no known competing financial interests or personal relationships that could have appeared to influence the work reported in this paper.

NOMENCLATURE

SLS	structured light system
FVM	focus variation microscopy
I'	average intensity
I''	intensity modulation
$\emptyset$	phase obtained after solving the phase shifted patterns
$k(u,v)$	location of point in 3D dataset
$\Phi(u,v)$	absolute phase
R	rotation matrix
T	Translation vector
m,n	point cloud datasets
d	distance to points in the chosen cross-section
(x_1,y_1)	points in the chosen region
(x,y)	point on the required cross-section
$f(i,j)$	weights for all the chosen points
i,j	indices for the points x and y
R_a	arithmetic average of the surface roughness
z_0	mean of z_i from all cross sections
z_i	vertical coordinate of a point on the cross-section
W	Shapiro-Wilk test value
t	paired t-test value
$\bar{v}_1, \bar{v}_2$	mean of the two vectors of a dimension of M×N from two 3D data
PCC	Pearson's Correlation Coefficient

References

[1] T. Ngo, T. Kashani, G. Imbalzano, K. Nguyen, D. Hui. Additive manufacturing (3D printing): A review of materials, methods, applications and challenges. Compos. Part B Eng, 143 (2018), pp. 172–196

[2] D. Schniederjans. Adoption of 3D-printing technologies in manufacturing: A survey analysis. Int. J. Prod. Econ, 183 (2017), pp. 287–298

[3] S. Whitehead, A. Shearer, D Watts, N Wilson. Comparison of two stylus methods for measuring surface texture. Dent. Mater, 15 (2) (1999), pp. 79–86

[4] W. Wu. 3D printing of thermoplastic PI and interlayer bonding evaluation. Mater. Lett, 229 (2018), pp. 206–209

[5] D. Ahn, J. Kweon, J. Choi, S. Lee. Quantification of surface roughness of parts processed by laminated object manufacturing. J. Mater. Process. Technol, 212 (2) (2012), pp. 339–346

[6] D. Ahn, J. Kweon, S. Kwon, J. Song, S. Lee. Representation of surface roughness in fused deposition modeling. J. Mater. Process. Technol, 209 (2009), pp. 5593–5600

[7] K. Nemoto. Development of a roughness measurement standard with irregular surface topography for improving 3D surface texture measurement. Meas. Sci. Technol, 20 (8) (2009)

[8] R. Campbell, M. Martorelli, H. Lee. Surface roughness visualisation for rapid prototyping models. CAD Comput. Aided Des, 34 (10) (2002), pp. 717–725

[9] G. Al-Kindi, B. Shirinzadeh. An evaluation of surface roughness parameters measurement using vision-based data. Int. J. Mach. Tools Manuf, 47 (3–4) (2007), pp. 697–708
[10] S. Leelawattananon. Surface Roughness measurement application using multi-frame techniques. International Conference on Computer 2015, pp. 86–91
[11] B. Bhushan. Modern Tribology Handbook 2000, 2(5)
[12] H. Mccormick, K. Duho. A Brief History of the Development of 2-D Surface Finish Characterization and More Recent Developments in 3-D Surface Finish Characterization. Society of Manufacturing Engineers 2007
[13] A. Boschetto, V. Giordano, F. Veniali. Modelling micro geometrical profiles in fused deposition process. Int. J. Adv. Manuf. Technol, 61 (9–12) (2012), pp. 945–956
[14] A. Thompson, I. Maskery, R. Leach. X-ray computed tomography for additive manufacturing: A review. Meas. Sci. Technol, 27 (7) (2016), pp. 072001
[15] C. Tay, S. Wang, C. Quan, H. Shang. In situ surface roughness measurement using a laser scattering method. Opt. Commun, 218 (1–3) (2003), pp. 1–10
[16] M. Launhardt. Detecting surface roughness on SLS parts with various measuring techniques. Polym Test, 53 (2016), pp. 217–226
[17] J. Chambers, J. Sabatier. Recent advances in utilizing acoustics to study surface roughness in agricultural surfaces. Appl. Acoust, 63 (7) (2002), pp. 795–812
[18] V. Nadimpalli, L. Yang, P. Nagy. In-situ interfacial quality assessment of Ultrasonic Additive Manufacturing components using ultrasonic NDE. NDT E Int, 93 (2018), pp. 117–130
[19] S. Coker, Y. Shin. In-process control of surface roughness due to tool wear using a new ultrasonic system. Int. J. Mach. Tools Manuf, 36 (3) (1996), pp. 411–422
[20] C. Poon, B. Bhushan. Comparison of surface roughness measurements by stylus profiler, AFM and non-contact optical profiler. Wear, 190 (1) (1995), pp. 76–88
[21] G. Chinga, P. Johnsen, R. Dougherty, E. Berli, J. Walter. Quantification of the 3D microstructure of SC surfaces. J. Microsc, 227 (3) (2007), pp. 254–265
[22] H. Zhong, Z. Lei, T. Jia, M. Xue, S. Xiao. Evaluation of three-dimensional surface roughness parameters based on digital image processing. Int. J. Adv. Manuf. Technol, 40 (3–4) (2009), pp. 342–348
[23] Z. Yilbas. Optical method and neural network for surface roughness measurement and surface pattern classification. Doctoral dissertation 1998
[24] R. Kumar, P. Kulashekar, B. Dhanasekar, B. Ramamoorthy. Application of digital image magnification for surface roughness evaluation using machine vision. Int. J. Mach. Tools Manuf, 45 (2) (2005), pp. 228–234
[25] Y. Fuh, K. Hsu, J. Fan. Roughness measurement of metals using a modified binary speckle image and adaptive optics. Opt. Lasers Eng, 50 (3) (2012), pp. 312–316
[26] B. Zhang, J. Ziegert, F. Farahi, A. Davies. In situ surface topography of laser powder bed fusion using fringe projection. Addit. Manuf, 12 (2016), pp. 100–107
[27] L. Newton, N. Senin, C. Gomez, R. Danzl, F. Helmli, L. Blunt, R. Leach. Areal topography measurement of metal additive surfaces using focus variation microscopy. Additive Manufacturing, 25 (2019), pp. 365-389
[28] M. Tomov, M. Kuzinovski, P. Cichosz. Modeling and prediction of surface roughness profile in longitudinal turning. Journal of Manufacturing Processes, 24 (2016), pp. 231-255
[29] D. Malacara. Optical shop testing. John Wiley & Sons, 59 (2007), pp. 557-560
[30] P. Besl, N. McKay. Method for registration of 3-D shapes. In Sensor fusion IV: control

paradigms and data structures. International Society for Optics and Photonics, 1611 (1992), pp. 586-606
[31] S. Rusinkiewicz, M. Levoy. Efficient variants of the ICP algorithm. In 3dim, 11 (2001), pp. 45-152
[32] B. Li, S. Zhang. Flexible calibration method for microscopic structured light system using telecentric lens. Opt. Express, 23 (20) (2015), pp. 25795–25803
[33] N. Roussopoulos, S. Kelley, F. Vincent. Nearest neighbor queries. ACM sigmod record, 24 (2) (1995), pp. 71-79
[34] W. Shapiro. An analysis of variance test for normality (complete samples). Biomerika, 52 (3/4) (1965), pp. 591–611
[35] H. David, J. Gunnink. The Paired T Test Under Artificial Pairing. Am. Stat, 51 (1) (1997), pp. 9–12
[36] F. Wilcoxon. Individual Comparisons by Ranking Methods. Biometrics Bulletin, 1 (6) (2018), pp. 80–83
[37] K. Pearson. LIII. On lines and planes of closest fit to systems of points in space. The London, Edinburgh, and Dublin Philosophical Magazine and Journal of Science, 2 (11) (1901), pp. 559-572
[38] M Schmidt, K. Rothman. Mistaken inference caused by reliance on and misinterpretation of a significance test. International journal of cardiology, 177 (3) (2014), pp. 1089-1090
[39] R. Wasserstein, A. Schirm, N. Lazar. Moving to a World Beyond “p< 0.05”. The American Statistician, 73 (2019), pp.1-19
[40] N. Smirnov. Table for estimating the goodness of fit of empirical distributions. The annals of mathematical statistics, 19 (2) (1948), pp. 279-328
[41] H. Mann, D. Whitney. On a test of whether one of two random variables is stochastically larger than the other. The annals of mathematical statistics, 1 (1947), pp. 50-60
[42] J. Zhang, A. Chaudhari, H. Wang. Surface quality and material removal in magnetic abrasive finishing of selective laser melted 316L stainless steel. Journal of Manufacturing Processes, 45 (2019), pp. 710-719
[43] G. Kiswanto, D. Zariatin, T. Ko. The effect of spindle speed, feed-rate and machining time to the surface roughness and burr formation of Aluminum Alloy 1100 in micro-milling operation. Journal of Manufacturing Processes, 16 (4) (2014), pp. 435-50
[44] G. Saurav. Advances in the surface defect machining (SDM) of hard steels. Wear, 302 (2013), pp.1124-1135